Published in IET Radar, Sonar and Navigation
Received on 9th March 2009
Revised on 14th August 2009
doi: 10.1049/iet-rsn.2009.0053

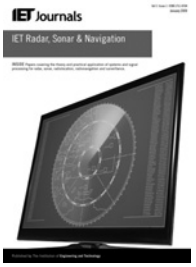

ISSN 1751-8784

Passive bistatic noise radar using DVB-T signals

J. Raout[1] *A. Santori*[1] *E. Moreau*[2]

[1]*MorphoAnalysis in Signal processing Lab., Research Center of the French Air Force, 13 661 Salon de Provence, France*
[2]*University of Sud Toulon Var, ISITV, LSEET UMR-CNRS 6017 av. G. Pompidou, BP 56, 83162 La Valette du Var, Cedex, France*
E-mail: jraout@sfr.fr

Abstract: This study presents a new approach to passively detect targets using noise-like emitters of opportunity. This method combines the Wiener filtering to achieve clutter rejection and a proposed adaptation to noise-like signals of the amplitude and phase estimation (APES) method. This theoretical approach is confirmed by the detection of a helicopter by a bistatic radar using a digital video broadcasting terrestrial (DVB-T) transmitter.

1 Introduction

Radars using transmitters of opportunity are inherently passive bistatic radars. The passivity of bistatic radars offers advantages, namely: low cost, low weight and enhanced radar cross-section for certain geometries. Moreover, stealth operations are possible since the receiver is totally passive [1].

Such radars have already been studied. Signals provided by FM radio broadcast [2], satellites [3, 4] and global system for mobile communications (GSM) base stations [5, 6] have been considered. Arguments for the selection of the transmitter type include spatial and time coverage, power, central-frequency and bandwidth of the emitted signal and shape of the ambiguity function. The bandwidth dictates the achievable range-resolution and the shape of the ambiguity function is decisive in determining the detection performance of the radar. In particular, signals from digital modulations (GSM, DVB-T) have much less range and Doppler ambiguities than other modulations [7], which makes them more suitable for passive radar.

In this paper, we will consider DVB-T transmitters. This kind of emitter of opportunity delivers a noise-like signal in the bandwidth associated to each channel.

Beside all the advantages previously described, noise-like signals ambiguity function presents no side lobes (just noise floor), and behave favourably against electronic countermeasures (anti-radar missile (ARM) and jamming). They also exhibit better performance in low probability of interception (LPI) and low probability of exploiting (LPE). In the electromagnetic compatibility (EMC) domain, better interference immunity and the possibility of using many radars simultaneously within the same area is expected.

Passively detecting the echo created by a target illuminated by such a transmitter implies to reject ground clutter. We will use the Wiener filtering in this frame before applying a proposed adapted version to noise-like signals of the amplitude and phase estimation (APES) method. This method is more general than the direct data domain (D^3) already used for passive detection [8] and allows a localisation in both temporal and spatial domains simultaneously compared to other methods where two steps are necessary [9].

The paper is organised as follows. Section 2 depicts the reference signal model, namely, DVB-T signal characteristics and the received signal model, made of the signal of interest (the target), clutter and noise. Section 3 then presents both clutter rejection through the Wiener filtering and its optimisation thanks to the study of the range-Doppler diagram. Section 4 is dedicated to the adaptation to noise-like signals of the APES method.

Finally, Section 5 describes results of the bistatic passive detection of a real target, using DVB-T transmitters of opportunity.

Notations: *, ^{T}, †, $\hat{}$ represent, respectively, the conjugate, transpose, Hermitian transpose and estimate of a vector/matrix.

The element corresponding to the column c and row l of a matrix $\boldsymbol{M}$ will be represented by $\boldsymbol{M}_{lc}$, its line index l by $\boldsymbol{M}_l$.

The C first values of a vector $\boldsymbol{v}$ will be represented by $\boldsymbol{v}_C$, its lth element by v_l, the portion of this vector between elements i and j by $\boldsymbol{v}_{i:j}$.

The identity matrix with dimension N will be written $\boldsymbol{I}_N$, $\boldsymbol{c}_C$ is the column vector with C unit elements, $\boldsymbol{0}_N$ is the column vector with N null elements, $\boldsymbol{l}_L$ is the row vector with L unit elements.

The Kronecker product is represented by $\otimes$, the Hadamard product by $\circ$. If we consider an $N \times M$ matrix $\boldsymbol{A}$, the vec-function of $\boldsymbol{A}$ is written as vec($\boldsymbol{A}$) and is obtained by stacking the columns to get an $NM \times 1$ vector.

2 Signals models

2.1 Transmitted DVB-T signal characteristics

As mentioned in the introduction, several kinds of transmitters of opportunity are potentially available on a battlefield. We decide to focus on DVB-T transmitters because of:

- the ubiquitous spatial coverage of the transmitters,
- the permanency in time,
- the large bandwidth (7.61 MHz for 8 K mode) leading to a range resolution of about 20 m to be compared with FM radio, 1.5 to 6 km, digital audio broadcasting (DAB), 200 m or analog television, 3 km,
- the importance of the equivalent isotropic radiated power (EIRP, several kilowatts),
- the possible high rate compression.

The general expression of an orthogonal frequency division multiplex (OFDM) frame, delivered by DVB-T emitters and made of subcarriers either dedicated to data, channel equalisation (scattered and continuous pilots), or signalisation (transmission parameters signalling (TPS)), is

$$x(t) = \mathrm{e}^{2\mathrm{j}\pi f_0 t} \sum_{p=0}^{P-1} \sum_{q=0}^{Q-1} \sum_{r=0}^{N_{\mathrm{sc}}-1} x_{p,q,r} \Psi_{p,q,r}(t) \qquad (1)$$

with f_0 the central frequency, p the index of P frames number, q the index of Q OFDM symbols and r the index of N_{sc} subcarriers, $x_{p,q,r}$ the complex data and

$$\Psi_{p,q,r}(t) = \begin{cases} \mathrm{e}^{2\mathrm{j}\pi \frac{r}{T_u}(t - T_p - (pQ+q)T_{\mathrm{s}})} \\ \quad \text{with } (pQ+q)T_{\mathrm{s}} \le t \le (pQ+q+1)T_{\mathrm{s}} \\ 0, \quad \text{elsewhere} \end{cases}$$

Table 1 provides the main characteristics of OFDM signals.

These parameters lead to a modulation exhibiting much less range and Doppler ambiguities than other modulations [7].

Fig. 1*a* presents the ambiguity function of a sampled OFDM signal

$$\chi_{\mathrm{x}}(\tau, \nu_{\mathrm{d}}) = \sum_{l} x\left(\frac{l}{f_{\mathrm{s}}}\right) x^*\left(\frac{l}{f_{\mathrm{s}}} - \tau\right) \mathrm{e}^{-\mathrm{j}2\pi\nu_{\mathrm{d}} l} \qquad (2)$$

with τ the delay corresponding to a range cell, $\nu_{\mathrm{d}} = f_{\mathrm{d}}/f_{\mathrm{s}}$ the reduced Doppler frequency, f_{d} the Doppler frequency, f_{s} the sampling frequency and $x(l/f_{\mathrm{s}})$ the lth sample of the reference signal.

The ambiguities are due to the cyclic prefix or guard interval and the presence of signalling subcarriers [10].

One can understand the interesting thumbtack-like shape of the various peaks considering the flatness of the OFDM spectrum in Fig. 1*b*.

2.2 Received signal model

Let us consider a sampled space–time signal $\boldsymbol{Y}$, made of clutter, potential target and noise, received by a sparse array

Table 1 Main parameters of OFDM signal (8 k mode)

Parameters	8 k mode
total number of subcarriers (N_{sc})	6817
data subcarriers	6048
scattered pilot cells	524
continual pilot carriers	177
TPS	68
symbol duration (T_u)	896 μs
carrier spacing	1116 Hz
bandwidth	7,61 MHz
guard interval (T_p)	$\frac{T_u}{4}$, $\frac{T_u}{8}$, $\frac{T_u}{16}$ or $\frac{T_u}{32}$
time for a symbol (T_{s})	$T_u + T_p$
modulation	QPSK, 16-QAM, or 64-QAM in our case

IET Radar Sonar Navig., 2010, Vol. 4, Iss. 3, pp. 403–411
doi: 10.1049/iet-rsn.2009.0053

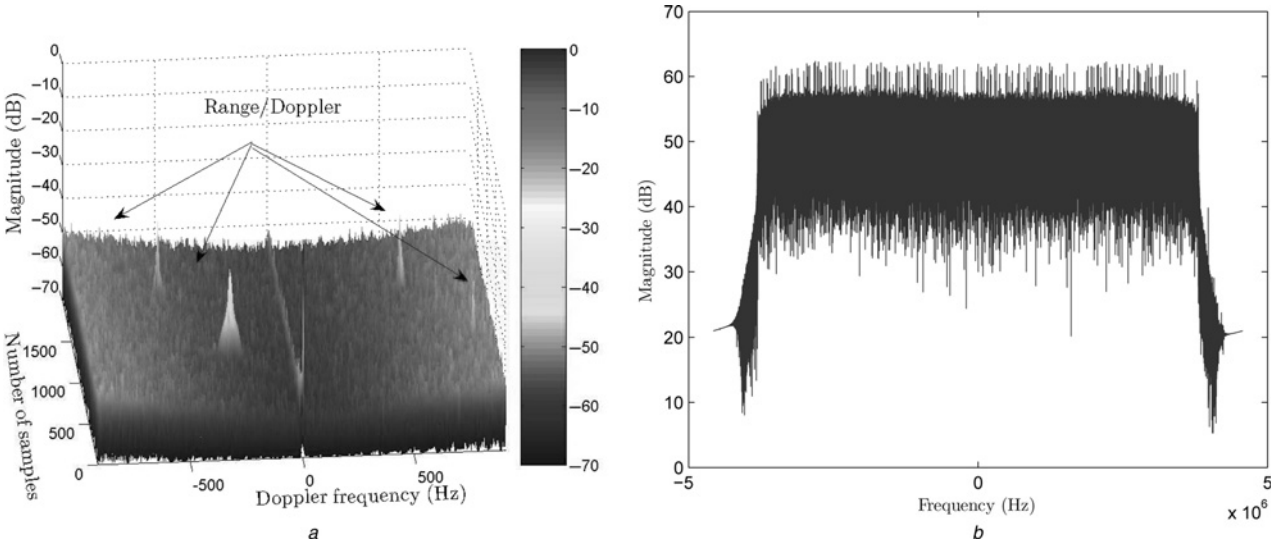

Figure 1 *OFDM signal ambiguity function (a) and DVB-T spectrum (b)*

antenna made of N_s elements, during a coherent integration time T_{ci} corresponding to N_d samples, so that $T_{ci} = N_d/f_s$. The inter-element spacing between the $i+1$th antenna element and the previous one is represented by $d_{i+1,i}$ and the carrier wavelength by λ.

The various components of the received signal are defined by their amplitude, delay compared to the direct path, reduced Doppler frequency and associated steering vector in the temporal domain and direction of arrival and associated steering vector in the spatial domain.

The general expression of a temporal steering vector in the direction of the reduced Doppler frequency ν_d is given by

$$\begin{aligned} \boldsymbol{s}_d(\nu_d) &= [1, e^{j2\pi\nu_d}, \ldots, e^{j2\pi\nu_d(N_d-1)}]^T \\ &= [1, z_d(\nu_d), \ldots, z_d^{N_d-1}(\nu_d)]^T \end{aligned} \tag{3}$$

where $z_d(\nu_d)$ stands for the temporal phase shift from one sample to another due to the motion of the considered component.

In the case of a sparse array (used for real measurements), the spatial steering vector in the direction of arrival θ is

$$\begin{aligned} \boldsymbol{s}_s(\theta) &= \left[1, e^{j2\pi(\sin(\theta)/\lambda)d_{2,1}}, \ldots, e^{j2\pi(\sin(\theta)/\lambda)\sum_{i=0}^{N_s-1} d_{i+1,i}}\right]^T \\ &= \left[z_{s_{1,0}}(\theta), z_{s_{2,1}}(\theta), \ldots, \prod_{i=0}^{N_s-1} z_{s_{i+1,i}}(\theta)\right]^T \end{aligned} \tag{4}$$

where $z_{s_{i+1,i}}(\theta)$ stands for the spatial phase shift from the element $i+1$ of the antenna to the previous element. By convention, $z_{s_{1,0}}(\theta)$ is chosen equal to 1.

The space–time steering vector is deduced from both spatial and temporal steering vectors

$$\boldsymbol{s}(\theta, \nu_d) = \boldsymbol{s}_d(\nu_d) \otimes \boldsymbol{s}_s(\theta) \tag{5}$$

The clutter signal $\boldsymbol{Y}_c$ is assumed to be made of the total contribution of N_r interfering range cells, creating multipaths. Each range cell is made of $N_{r;p}$ contributing clutter patches with complex amplitude $\alpha_{r;p}$, delay $\tau_r = r/f_s$, spatial steering vector $\boldsymbol{s}_s(\theta_p)$ linked to the angle θ_p. It is not necessary to take into account the temporal steering vector if we neglect internal clutter motion ($\nu_{d_{r;p}} = 0$ and $\boldsymbol{s}_d(\nu_{d_{r;p}}) = 1_{N_d} \forall r \in [1, \ldots, N_r]$ and $\forall p \in [1, \ldots, N_{r;p}]$) so that

$$\boldsymbol{Y}_c = \sum_{r=1}^{N_r} \sum_{p=1}^{N_{r;p}} \alpha_{r;p} \boldsymbol{s}_s(\theta_p) \boldsymbol{x}^T(-\tau_r) \tag{6}$$

with the general expression

$$\boldsymbol{x}(-\tau_r) = \left[x\left(\frac{1-r}{f_s}\right), x\left(\frac{2-r}{f_s}\right), \ldots, x\left(\frac{N_d-r}{f_s}\right)\right]^T \tag{7}$$

The signal is also supposed to be made of a target with complex amplitude α and located at angle θ, reduced Doppler frequency ν_d and bistatic delay τ.

Noise is represented by $\boldsymbol{N}$.

The general expression of the received signal is

$$\begin{aligned}\boldsymbol{Y} &= \boldsymbol{Y}_{\mathrm{c}} + \alpha \boldsymbol{s}_s(\theta)(\boldsymbol{x}(-\tau) \circ \boldsymbol{s}_d(\nu_{\mathrm{d}}))^{\mathrm{T}} + \boldsymbol{N} \\ &= \boldsymbol{Y}_{\mathrm{c}} + \alpha(\mathbf{c}_{N_s} \otimes \boldsymbol{x}^{\mathrm{T}}(-\tau)) \circ (\boldsymbol{s}_s(\theta) \otimes \boldsymbol{s}_d^{\mathrm{T}}(\nu_{\mathrm{d}})) + \boldsymbol{N} \\ &= \boldsymbol{Y}_{\mathrm{c}} + \alpha \boldsymbol{X}(-\tau) \circ (\boldsymbol{s}_s(\theta) \otimes \boldsymbol{s}_d^{\mathrm{T}}(\nu_{\mathrm{d}})) + \boldsymbol{N} \end{aligned} \tag{8}$$

3 Clutter rejection

3.1 Principle of the Wiener filtering

One of the main challenges to achieve target detection is to reject clutter ($\boldsymbol{Y}_{\mathrm{c}}$). In order to reach this goal, and under the assumption of a static clutter, the Wiener filtering of the signal received on each antenna is proposed.

If, to begin with, we assume that all the N_r first range cells are contributing to the global clutter, and since the direct path corresponds, in general, to the main contribution of the clutter, and if we consider, $Y_{c_{i,l}}$, the lth sample received from clutter on the ith antenna, one can write

$$\begin{aligned} Y_{c_{i,l}} &= \sum_{r=1}^{N_r} \sum_{p=1}^{N_{r,p}} \alpha_{r,p} \prod_{k=1}^{i-1} z_{s_{k+1,k}}(\theta_p) x\left(\frac{l-r+1}{f_{\mathrm{s}}}\right) \\ &= \sum_{r=1}^{N_r} x\left(\frac{l-r+1}{f_{\mathrm{s}}}\right) \sum_{p=1}^{N_{r,p}} \alpha_{r,p} \prod_{k=0}^{i-1} z_{s_{k+1,k}}(\theta_p) \\ &= \left[\sum_{p=1}^{N_{1,p}} \alpha_{1,p} \prod_{k=0}^{i-1} z_{s_{k+1,k}}(\theta_p), \ldots, \sum_{p=1}^{N_{N_r,p}} \alpha_{N_r,p} \prod_{k=0}^{i-1} z_{s_{k+1,k}}(\theta_p)\right] \\ &\quad \times \begin{bmatrix} x\left(\frac{l}{f_{\mathrm{s}}}\right) \\ \vdots \\ x\left(\frac{l-N_r+1}{f_{\mathrm{s}}}\right) \end{bmatrix} \end{aligned}$$

$$Y_{c_{i,l}} = \boldsymbol{a}_i^{\mathrm{T}} \boldsymbol{x}_{l+N_r:l+1}(-\tau_{N_r}) \tag{9}$$

The objective of the Wiener filtering is, in this case, to estimate, for each antenna, $\boldsymbol{a}_i$, the vector containing the N_{r} amplitudes of the clutter from each interfering range cell made of the contribution of the various clutter patches. The estimated clutter $\hat{Y}_{\mathrm{c}}$ is then subtracted from the received signal.

The theoretical expression for the N_{r} coefficients related to the ith antenna is

$$\boldsymbol{a}_i = \boldsymbol{R}_{\boldsymbol{x}}^{-1} \boldsymbol{r}_{\boldsymbol{x}\boldsymbol{Y}_i} \tag{10}$$

The expression of both the covariance matrix of the reference signal and the cross-covariance vector of the received signal and the reference one are, respectively

$$\boldsymbol{R}_{\boldsymbol{x}} = E\{\boldsymbol{x}\boldsymbol{x}^{\dagger}\} \tag{11}$$

and

$$\boldsymbol{r}_{\boldsymbol{x}\boldsymbol{Y}_i} = E\{Y_{i,l}^{*}\boldsymbol{x}\} \tag{12}$$

In practice, the estimation of these statistical elements is obtained using

$$\hat{\boldsymbol{R}}_{\boldsymbol{x}} = \frac{1}{N_{\mathrm{e}}} \sum_{l=N_{\mathrm{r}}}^{N_{\mathrm{e}}+N_{\mathrm{r}}-1} \boldsymbol{x}_{l+N_{\mathrm{r}}:l+1}(-\tau N_{\mathrm{r}}) \boldsymbol{x}_{l+N_{\mathrm{r}}:l+1}^{\dagger}(-\tau N_{\mathrm{r}}) \tag{13}$$

and

$$\hat{\boldsymbol{r}}_{\boldsymbol{x}\boldsymbol{Y}_i} = \frac{1}{N_{\mathrm{e}}} \sum_{l=N_{\mathrm{r}}}^{N_{\mathrm{e}}+N_{\mathrm{r}}-1} Y_{i,l}^{*} \boldsymbol{x}_{l+N_{\mathrm{r}}:l+1}(-\tau N_{\mathrm{r}}) \tag{14}$$

The number N_{e} of samples used for the estimation corresponds to the assumed stationarity of the signals (see Table 2).

3.2 Range-Doppler diagram

The effectiveness of the Wiener filtering can be verified by representing the range-Doppler diagram, a generalisation of the input delay spread function, before and after the processing.

Table 2 Helicopter detection: configuration parameters

Acquisition parameters							
$\tilde{N}_d$	74	N_{s}	4	S	2^{13}	T_{ci}	66 ms
N_{e}		8448		N_g		100 over 600 main contributors	
Emitter							
EIRP		20 kW		Central frequency		562 MHz	
Target							
Type of target		Fennec helicopter		Direction of arrival (θ)		22°	
Doppler frequency (f_{d})		−162.5 Hz		Reduced Doppler frequency ($\tilde{\nu}_{\mathrm{d}}$)		−0.14	
Bistatic distance ($c\tau$)		17.5 km		Range cell (τf_{s})		535	

doi: 10.1049/iet-rsn.2009.0053

The range-Doppler diagram is defined for each antenna i by

$$\chi_{Y_i x}(\tau, \nu_d) = \sum_l Y_i\left(\frac{l}{f_s}\right) x^*\left(\frac{l}{f_s} - \tau\right) e^{-j2\pi\nu_d l} \quad (15)$$

Fig. 2 provides an example of the diagram obtained from real measurements (for the helicopter detection). This figure allows us to verify the hypothesis of a static clutter, the clutter ridge being concentrated around $f_d = 0$ Hz, before the Wiener filtering. One can also see on this figure that the Wiener filtering, applied with $N_e = 8448$, is able to reject ground clutter. The iteration k corresponds to the rejection of the clutter between range cell $200(k-1)+1$ and range cell 200 k. The value 200 is an example. It allows to study the 600 first range cells with three steps and to decrease the computational load necessary to reject the clutter with a single step.

Furthermore, this figure illustrates the rejection of Doppler side lobes.

One can also note that the computational load associated to the Wiener filtering is directly linked to the length of the filter N_r. In order to improve the processing by decreasing this size, it can be interesting to select the $N_g \ll N_r$ main scatterers.

The study of the range-Doppler diagram lead to choose N_g in an optimal way.

Instead of considering (9), one can now apply the Wiener filtering to

$$\left[x\left(\frac{l-n_1}{f_s}\right),\ x\left(\frac{l-n_2}{f_s}\right),\ \ldots,\ x\left(\frac{l-n_{N_g}}{f_s}\right)\right]^T \quad (16)$$

Each value n_r, $1 \le r \le N_g$, corresponds to the delay of the rth multipath, considered as a strong interferer.

Fig. 2, for example, was in fact obtained by selecting $N_g = 100$ main interfering range cells over 200 for each iteration.

4 Generalisation of the APES method to noise-like signals

In the case of a bistatic radar exploiting a noise-like signal, a way to adapt the APES method [11–13] is to work on the mixing product defined for each range r associated to the delay τ by

$$\boldsymbol{Y}_m(\tau) = \boldsymbol{Y}(\tau) \circ (\mathbf{c}_{N_s} \otimes \boldsymbol{x}^\dagger) = \boldsymbol{Y}(\tau) \circ \boldsymbol{X}^* \quad (17)$$

In an analogue way, we will no longer consider the reference signal or the noise signal but their mixed version, $\boldsymbol{X}_m$ and $\boldsymbol{N}_m(\tau)$.

Since the target of interest induces a Doppler frequency that is much smaller than the sampling frequency, the signal can be low-pass filtered and subsampled as suggested in [14]. The subsampling factor will be noted S. Note that this subsampling does not affect the range-resolution of the radar.

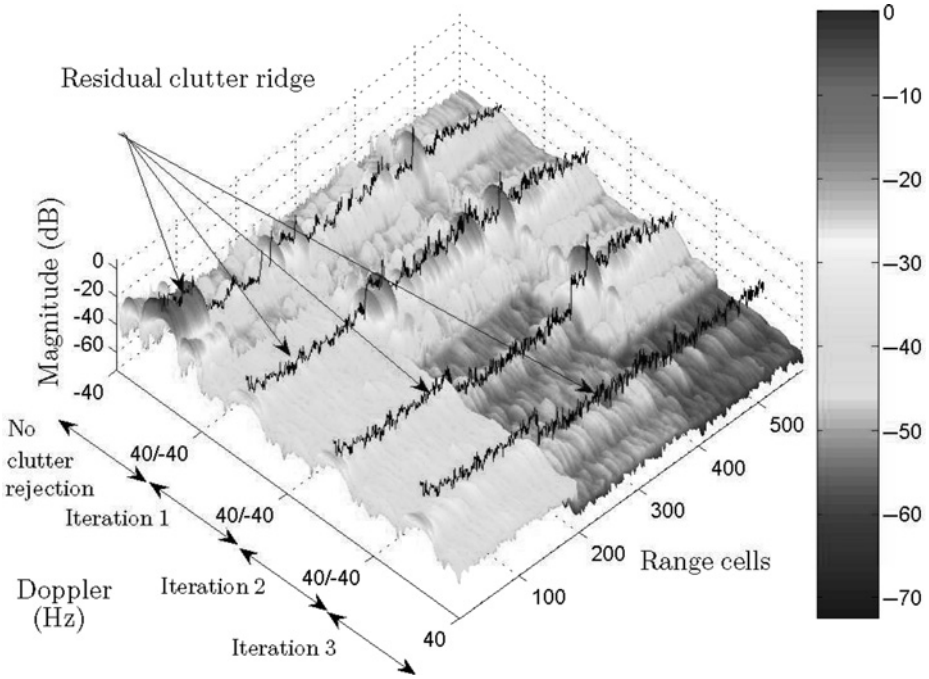

Figure 2 *Range-Doppler diagram before and after iterative Wiener filtering*

The reduced Doppler frequency after this processing will be noted $\tilde{\nu}_{\mathrm{d}} = \nu_{\mathrm{d}} S$.

Low-pass filtering and subsampling play an important role in the adaptation of the APES method to noise-like signal. Both the demodulation, represented by the Hadamard product of a delayed version, regarding the considered range cell, of the received signal by the reference one (see (17)) and low-pass filtering plus subsampling allow the noise-like signal to get closer to a Doppler shifted pulse with a low level of amplitude fluctuations.

This processing is associated to the subsampling and low-pass filtering matrix

$$\boldsymbol{S}(\nu_{\mathrm{d}}) = \mathrm{e}^{-\mathrm{j}\pi(S-1)\nu_{\mathrm{d}}} \frac{\sin(\pi\nu_{\mathrm{d}})}{\sin(\pi\tilde{\nu}_{\mathrm{d}})} \begin{bmatrix} \boldsymbol{c}_S & \boldsymbol{0}_S & \cdots & \cdots & \boldsymbol{0}_S \\ \boldsymbol{0}_S & \boldsymbol{c}_S & \boldsymbol{0}_S & \cdots & \boldsymbol{0}_S \\ \vdots & \ddots & \ddots & \ddots & \vdots \\ \vdots & \ddots & \ddots & \ddots & \vdots \\ \boldsymbol{0}_S & \cdots & \cdots & \boldsymbol{0}_S & \boldsymbol{c}_S \end{bmatrix}$$
$$= \iota(\nu_{\mathrm{d}}) \boldsymbol{I}_{N_d/S} \otimes \boldsymbol{c}_S \tag{18}$$

The correction by the coefficient

$$\iota(\nu_{\mathrm{d}}) = \frac{1}{\sum_{S-1}^{k=0} \mathrm{e}^{2\mathrm{j}\pi k\nu_{\mathrm{d}}}} \tag{19}$$

is necessary to compensate the effect of subsampling on the temporal steering vector. It yields

$$\boldsymbol{S}^{\mathrm{T}}(\nu_{\mathrm{d}}) \boldsymbol{s}_{\mathrm{d}}(\nu_{\mathrm{d}}) = \tilde{s}_{\mathrm{d}}(\tilde{\nu}_{\mathrm{d}}) \tag{20}$$

The mixed signal defined in (17), for example, will now be replaced by

$$\begin{aligned} \hat{\boldsymbol{Y}}(\tau, \nu_{\mathrm{d}}) &= \boldsymbol{Y}_m(\tau) \boldsymbol{S}(\nu_{\mathrm{d}}) \\ &= \iota(\nu_{\mathrm{d}}) \boldsymbol{Y}_m(\tau) \boldsymbol{S} \\ &= \iota(\nu_{\mathrm{d}}) \hat{\boldsymbol{Y}}(\tau) \end{aligned} \tag{21}$$

One can see on the previous equation that it is not necessary to take into account a different mixed, low-pass filtered and subsampled signal $\hat{\boldsymbol{Y}}(\tau, \nu_{\mathrm{d}})$ for each temporal direction but to work with $\hat{\boldsymbol{Y}}(\tau)$ and to apply the correction.

$\hat{\boldsymbol{X}}$ and $\hat{\boldsymbol{N}}(\tau)$ would be defined in the same way from $\boldsymbol{X}_m$ and $\boldsymbol{N}_m(\tau)$, respectively.

The number of processed blocks, made of subsampled and low-pass filtered data, N_{d}/S will be noted $\tilde{N}_{\mathrm{d}}$.

Considering the mixed, low-pass filtered and subsampled signals, the purpose is now to estimate $\alpha(\tau, \theta, \tilde{\nu}_{\mathrm{d}})$ so that

$$\hat{\boldsymbol{Y}}(\tau) = \alpha(\tau, \theta, \tilde{\nu}_{\mathrm{d}}) \hat{\boldsymbol{X}} \circ (\tilde{\boldsymbol{s}}_s(\theta) \tilde{\boldsymbol{s}}_{\mathrm{d}}^{\mathrm{T}}(\tilde{\nu}_{\mathrm{d}})) + \hat{\boldsymbol{N}}(\tau) \tag{22}$$

To facilitate readers understanding, the reference to the range cell (τ) and the spatio-temporal direction (θ, $\tilde{\nu}_{\mathrm{d}}$) will be suppressed.

Applying the APES method implies to work with $\tilde{\boldsymbol{\upsilon}}_{i;l}$

$$\tilde{\boldsymbol{\upsilon}}_{i;l} = \mathrm{vec}(\hat{\boldsymbol{Y}}_{i:i+M_s-1,l:l+\tilde{M}_d-1}) \tag{23}$$

and

$$\hat{\Upsilon} \triangleq [\tilde{\boldsymbol{\upsilon}}_{1;1}, \ \ldots, \ \tilde{\boldsymbol{\upsilon}}_{L_s;1}, \ \tilde{\boldsymbol{\upsilon}}_{1;2}, \ \ldots, \ \tilde{\boldsymbol{\upsilon}}_{L_s;\tilde{L}_d}] \tag{24}$$

The values of M_s, $\tilde{M}_d$, L_s and $\tilde{L}_d$ are chosen so that $\hat{\Upsilon}$ is a square matrix ($L_s\tilde{L}_d = M_s\tilde{M}_d$). In addition, the number of antenna elements of the sparse array being small ($N_s = 4$), M_s is chosen equal to N_s leading to $L_s = 1$ ($L_s = N_s - M_s + 1$).

Once the integration time and the subsampling factor are chosen and using $\tilde{L}_d = \tilde{N}_d - \tilde{M}_d + 1$, we obtain

$$\tilde{M}_d = \frac{\tilde{N}_d + 1}{N_s + 1} \tag{25}$$

Furthermore, we will note $\tilde{\boldsymbol{x}}$ the first column of the matrix $\hat{\boldsymbol{X}}^{\mathrm{T}}$.

This leads us to the optimisation problem

$$\min_{\boldsymbol{h},\alpha} \|\boldsymbol{h}^{\dagger}\hat{\Upsilon} - \alpha\tilde{\boldsymbol{x}}_{L_s\tilde{L}_d} \circ \tilde{\boldsymbol{s}}_{L_s\tilde{L}_d}\|^2 \tag{26}$$

or

$$\min_{\boldsymbol{h},\alpha} \sum_{i=1}^{L_s} \sum_{l=1}^{\tilde{L}_d} |\boldsymbol{h}^{\dagger}\tilde{\boldsymbol{\upsilon}}_{i;l} - \alpha\tilde{x}_l \tilde{z}_d^{l-1} \prod_{k=0}^{i-1} z_{s_{k+1,k}}|^2 \tag{27}$$

with the constraint

$$\boldsymbol{h}^{\dagger}(\tilde{\boldsymbol{x}}_{M_s\tilde{M}_d} \circ \tilde{\boldsymbol{s}}_{M_s\tilde{M}_d}) = 1 \tag{28}$$

$\boldsymbol{h} \in \mathbb{C}^{M_s\tilde{M}_d}$ is the vector containing the coefficients of the filter at the frequency (θ, $\tilde{\nu}_{\mathrm{d}}$) for the considered range cell.

Proposition 1 (Noise APES (NAPES filter)): The solution of the optimisation problem (26) under the constraint (28) is

$$\alpha = \boldsymbol{h}^{\dagger}\tilde{\boldsymbol{g}} \tag{29}$$

and

$$\boldsymbol{h} = \frac{\hat{\tilde{\Phi}}^{-1}\tilde{\boldsymbol{x}}^{sd}_{M_s\tilde{M}_d}}{(\tilde{\boldsymbol{x}}^{sd}_{M_s\tilde{M}_d})^{\dagger}\hat{\tilde{\Phi}}^{-1}\tilde{\boldsymbol{x}}^{sd}_{M_s\tilde{M}_d}} \tag{30}$$

IET Radar Sonar Navig., 2010, Vol. 4, Iss. 3, pp. 403–411
doi: 10.1049/iet-rsn.2009.0053

where

$$\tilde{\boldsymbol{g}} = \frac{1}{\|\tilde{\boldsymbol{x}}_{L_s\tilde{L}_d}\|^2}\sum_{i=1}^{L_s}\sum_{i=1}^{\tilde{L}_d}\tilde{\boldsymbol{v}}_{i;l}\tilde{x}_l^*\tilde{z}_d^{(l-1)}\prod_{k=0}^{i-1}z_{s_{k+1,k}}^* = \frac{1}{\|\tilde{\boldsymbol{x}}_{L_s\tilde{L}_d}\|^2}\hat{\Upsilon}(\tilde{\boldsymbol{x}}_{L_s\tilde{L}_d}^{sd})^* \quad (31)$$

$$\hat{\tilde{\Phi}} = \frac{1}{\|\tilde{\boldsymbol{x}}_{L_s\tilde{L}_d}\|^2}\left(\sum_{i=1}^{L_s}\sum_{l=1}^{\tilde{L}_d}\tilde{\boldsymbol{v}}_{i;l}\tilde{\boldsymbol{v}}_{i;l}^{\dagger}\right) - \tilde{\boldsymbol{g}}\tilde{\boldsymbol{g}}^{\dagger} = \frac{1}{\|\tilde{\boldsymbol{x}}_{L_s\tilde{L}_d}\|^2}\hat{\Upsilon}\hat{\Upsilon}^{\dagger} - \tilde{\boldsymbol{g}}\tilde{\boldsymbol{g}}^{\dagger} = \hat{\tilde{\Xi}} - \tilde{\boldsymbol{g}}\tilde{\boldsymbol{g}}^{\dagger} \quad (32)$$

$\tilde{\boldsymbol{x}}_{M_s\tilde{M}_d}^{sd}$ is obtained from the reference signal, mixed, lowpass filtered, subsampled and steered in the desired spatiotemporal direction

$$\tilde{\boldsymbol{x}}_{M_s\tilde{M}_d}^{sd} = \tilde{\boldsymbol{x}}_{M_s\tilde{M}_d} \circ \tilde{\boldsymbol{s}}_{M_s\tilde{M}_d} \quad (33)$$

and

$$\|\tilde{\boldsymbol{x}}_{L_s\tilde{L}_d}\|^2 = \sum_{i=1}^{L_s}\sum_{i=1}^{\tilde{L}_d}|\tilde{x}_l|^2 = L_s\sum_{l=1}^{\tilde{L}_d}|\tilde{x}_l|^2 \quad (34)$$

The demonstration is provided in the Appendix.

5 Application to real data

In [15–19] the optimum gaussian detector or adapted matched filter is adapted to single data set detection and

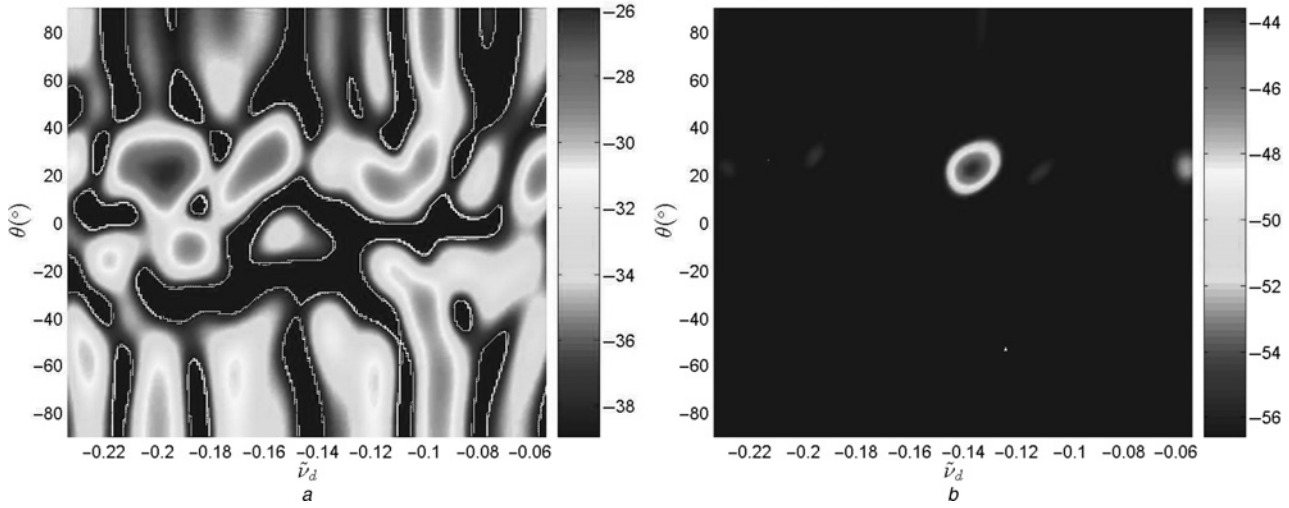

Figure 3 $\Lambda_{APES-MLED}$ *in the range cell of the target 535 before (a) and after (b) Wiener filtering*

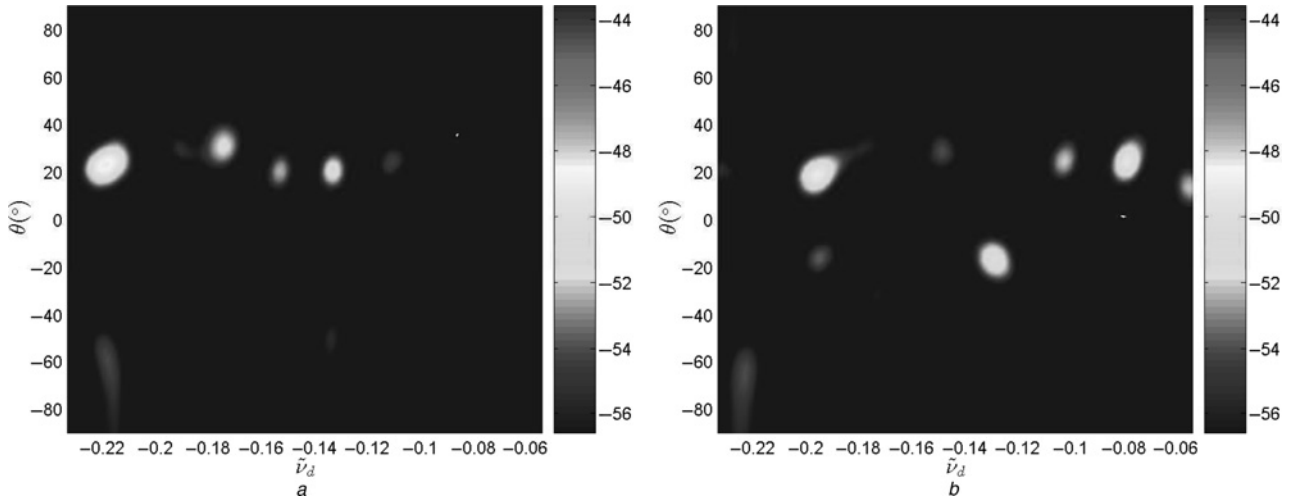

Figure 4 $\Lambda_{APES-MLED}$ *in the adjacent range cells 534 (a) and 536 (b)*

lead to the maximum likelihood estimation detector (MLED).

Considering the statistical hypothesis H_1 corresponding to the presence of a target, H_0 the statistical hypothesis corresponding to the presence of residual interference only and a defined threshold ζ, we propose to generalise this approach and to define the adapted version of the MLED test to noise-like signals

$$\Lambda_{\text{APES-MLED}} = \frac{|(\tilde{\boldsymbol{x}}^{sd}_{M_s\tilde{M}_d})^{\dagger}\hat{\tilde{\boldsymbol{\Phi}}}^{-1}\tilde{\boldsymbol{g}}|^2}{(\tilde{\boldsymbol{x}}^{sd}_{M_s\tilde{M}_d})^{\dagger}\hat{\tilde{\boldsymbol{\Phi}}}^{-1}\tilde{\boldsymbol{x}}^{sd}_{M_s\tilde{M}_d}} \underset{H_0}{\overset{H_1}{\lessgtr}} \zeta \qquad (35)$$

Table 2 provides the configuration parameters of the detection of a helicopter using the Eiffel Tower DVB-T emitter.

The reference signal was received on a dedicated omnidirectional antenna. Thanks to the sufficient signal to noise ratio, this signal was demodulated and resynthetised.

Figs. 3*a* and *b* present the statistical test estimated at range cell 535, respectively, before and after Wiener filtering.

Figs. 4*a* and *b* present the same statistical test estimated in adjacent range cells 534 and 536 after Wiener filtering.

If on the one hand only false alarms are visible in Fig. 3*a*, and if only range sidelobes appear in Figs. 4*a* and *b*, on the other hand the target clearly appears in Fig. 3*b* after Wiener filtering in range cell 535 corresponding to its bistatic range. Both the reduced Doppler frequency and angular position are correct.

6 Conclusion

We have shown in this paper how efficient the Wiener filtering could be in the frame of the rejection of ground clutter for a bistatic passive radar.

It has also been proved that the APES method could be generalised to noise-like signal leading to the detection of a real target even with a low-radar cross-section and important bistatic range.

7 Acknowledgment

The authors thank François Delaveau and François Pipon (Thales-communications, EDS/SPM/SBP, Colombes, France) for providing raw data.

8 References

[1] MELVIN W.L.: 'Issues in bistatic STAP'. Proc. 32nd Southeastern Symp. on System Theory, March 2000, pp. 17–21

[2] ZHENG H., LI F., LUO J., LU J.: 'Bistatic radar experiment based on FM broadcast transmitter'. Proc. IEEE Radar Conf., October 2004

[3] HORNER J., KUBIK K., MOJARRABI B., LONGSTAFF I.D., DONSKOI E., CHERNIAKOV M.: 'Passive bistatic radar sensing with LEOS based transmitters'. Proc. IGARSS 02, June 2002, vol. 1, pp. 438–440

[4] CHERNIAKOV M., ZENG T., PLAKIDIS E.: 'Galileo signal-based bistatic system for avalanche prediction'. Proc. IGARSS 03, July 2003, pp. 784–786

[5] TAN D.K.P., SUN H., LUI Y., LESTURGIE M., CHAN H.L.: 'Passive radar using global system for mobile communication signal: theory, implementation and measurements', *Proc. IEE Radar Sonar Navig.*, 2005, **152**, (3), pp. 116–123

[6] KUBICA M., KUBICA V., NEYT X., RAOUT J., ROQUES S., ACHEROY M.: 'Optimum target detection using emitters of opportunity'. Proc. IEEE Radar Conf., April 2006, pp. 417–424

[7] GRIFFITHS H.D., BAKER C.J.: 'Measurement and analysis of ambiguity functions of passive radar transmissions'. Proc. IEEE Radar Conf., May 2005, pp. 321–325

[8] RAOUT J.: 'Sea target detection using passive DVB–T based radar'. Proc. IEEE Radar Conf., September 2008, pp. 691–694

[9] PIPON F., DELAVEAU F., HEURGUIER D.: 'Une approche communication pour la détection passive de cibles mobiles', *Rev. Electr. Electron.*, January 2006, **1**, pp. 26–35

[10] SAINI R., CHERNIAKOV M.: 'DTV signal ambiguity function analysis for radar application', *IEE Proc. Radar Sonar Navig.*, 2005, **152**, (3), pp. 133–142

[11] LI J., STOICA P.: 'An adaptive filtering approach to spectral estimation and SAR imaging', *IEEE Trans. Signal Process.*, 1996, **44**, (2), pp. 1469–1484

[12] STOICA P., LI H., LI J.: 'A new derivation of the APES filter', *IEEE Signal Process. Lett.*, 1999, **6**, pp. 205–206

[13] STOICA P., LI H., LI J.: 'Amplitude estimation of sinusoidal signals: survey, new results and an application', *IEEE Trans. Signal Process.*, **200**, (48), pp. 338–352

[14] STEIN S.: 'Algorithms for ambiguity function processing', *IEEE Trans. Acoust., Speech Signal Process.*, 1981, **29**, (3), pp. 588–599

[15] ABOUTANIOS E., MULGREW B.: 'Assessment of single data set detection algorithms under template mismatch'. Proc. 2005 IEEE Int. Symp. on Signal Processing and Information Technology, 2005, pp. 269–274

doi: 10.1049/iet-rsn.2009.0053

[16] ABOUTANIOS E., MULGREW B.: 'A hybrid *STAP* approach for radar target detection in heterogeneous environments'. 14th European Signal Processing Conf. Eusipco 2006, September 2006

[17] ABOUTANIOS E., MULGREW B.: 'Evaluation of the single and two data set STAP detection algorithms using measured data'. Int. Geoscience and Remote Sensing Symp., July 2007, pp. 494–498

[18] ABOUTANIOS E., MULGREW B.: 'Heterogeneity detection for hybrid STAP algorithm'. Proc. IEEE Radar Conf., May 2008, pp. 1–4

[19] LIM C., MULGREW B., ABOUTANIOS E.: 'JDL–STAP for ground moving target detection'. Proc. IET Conf. on Radar Systems, October 2007

9 Appendix

Note: In the following proof the index$_i$ will correspond to antenna elements and the index$_l$ to samples.

Temporal and spatial phase shifts are defined in Section 2.2.

The mixed, low-pass filtered and subsampled version of the reference signal $\tilde{\boldsymbol{x}}$, and the parameters L_s, $\tilde{L}_d$, M_s and $\tilde{M}_d$ are defined in Section 4. The vector $\tilde{\boldsymbol{v}}_{i;l}$ is also defined in this section in (23).

Proof: Let us consider $I(\alpha, \boldsymbol{h})$ the quantity to be optimised under constraint in order to estimate the amplitude of the target α thanks to $\boldsymbol{h} \in \mathbb{C}^{M_s\tilde{M}_d}$ the vector containing the coefficients of the filter at the frequency $(\theta, \tilde{\nu}_d)$ for the considered range cell

$$\begin{aligned}
I(\alpha, \boldsymbol{h}) &= \sum_{i=1}^{L_s}\sum_{l=1}^{\tilde{L}_d} |\boldsymbol{h}^\dagger \tilde{\boldsymbol{v}}_{i;l} - \alpha\tilde{x}_l\tilde{z}_d^{l-1}\prod_{k=0}^{i-1} z_{s_{k+1,k}}|^2 \\
&= \sum_{i=1}^{L_s}\sum_{l=1}^{\tilde{L}_d}\left(\boldsymbol{h}^\dagger\tilde{\boldsymbol{v}}_{i;l} - \alpha\tilde{x}_l\tilde{z}_d^{l-1}\prod_{k=0}^{i-1} z_{s_{k+1,k}}\right) \\
&\quad\times\left(\tilde{\boldsymbol{v}}_{i;l}^\dagger\boldsymbol{h} - \alpha^*\tilde{x}_l^*\tilde{z}_d^{-(l-1)}\prod_{k=0}^{i-1} z_{s_{k+1,k}}^*\right) \\
&= \boldsymbol{h}^\dagger\sum_{i=1}^{L_s}\sum_{l=1}^{\tilde{L}_d}\tilde{\boldsymbol{v}}_{i;l}\tilde{\boldsymbol{v}}_{i;l}^\dagger\boldsymbol{h} + \sum_{i=1}^{L_s}\sum_{l=1}^{\tilde{L}_d}|\alpha|^2|\tilde{x}_l|^2 \\
&\quad - \alpha^*\boldsymbol{h}^\dagger\sum_{i=1}^{L_s}\sum_{l=1}^{\tilde{L}_d}\tilde{x}_l^*\tilde{z}_d^{-(l-1)}\prod_{k=0}^{i-1} z_{s_{k+1,k}}^*\tilde{\boldsymbol{v}}_{i;l} \\
&\quad - \alpha\sum_{i=1}^{L_s}\sum_{l=1}^{\tilde{L}_d}\tilde{x}_l\tilde{z}_d^{-(l-1)}\prod_{k=0}^{i-1} z_{s_{k+1,k}}\tilde{\boldsymbol{v}}_{i;l}^\dagger\boldsymbol{h}
\end{aligned}$$

Let us note

$$\hat{\tilde{\boldsymbol{\Xi}}} = \frac{1}{\|\tilde{\boldsymbol{x}}_{L_s\tilde{L}_d}\|^2}\sum_{i=1}^{L_s}\sum_{l=1}^{\tilde{L}_d}\tilde{\boldsymbol{v}}_{i;l}\tilde{\boldsymbol{v}}_{i;l}^\dagger \tag{36}$$

and

$$\begin{aligned}
\|\tilde{\boldsymbol{x}}_{L_s\tilde{L}_d}\|^2 &= \sum_{i=1}^{L_s}\sum_{l=1}^{\tilde{L}_d}|\tilde{x}_l|^2 \\
&= L_s\sum_{l=1}^{\tilde{L}_d}|\tilde{x}_l|^2
\end{aligned} \tag{37}$$

$$\begin{aligned}
I(\alpha, \boldsymbol{h}) &= \|\tilde{\boldsymbol{x}}_{L_s\tilde{L}_d}\|^2\boldsymbol{h}^\dagger\hat{\tilde{\boldsymbol{\Xi}}}\boldsymbol{h} + \|\tilde{\boldsymbol{x}}_{L_s\tilde{L}_d}\|^2(|\alpha|^2 - \alpha^*\boldsymbol{h}^\dagger\tilde{\boldsymbol{g}} - \alpha\tilde{\boldsymbol{g}}^\dagger\boldsymbol{h}) \\
&= \|\tilde{\boldsymbol{x}}_{L_s\tilde{L}_d}\|^2(\boldsymbol{h}^\dagger\hat{\tilde{\boldsymbol{\Xi}}}\boldsymbol{h} + |\alpha - \boldsymbol{h}^\dagger\tilde{\boldsymbol{g}}|^2 - |\boldsymbol{h}^\dagger\tilde{\boldsymbol{g}}|^2) \\
&= \|\tilde{\boldsymbol{x}}_{L_s\tilde{L}_d}\|^2(\boldsymbol{h}^\dagger(\hat{\tilde{\boldsymbol{\Xi}}} - \tilde{\boldsymbol{g}}\tilde{\boldsymbol{g}}^\dagger)\boldsymbol{h} + |\alpha - \boldsymbol{h}^\dagger\tilde{\boldsymbol{g}}|^2)
\end{aligned}$$

is minimal for

$$\alpha = \boldsymbol{h}^\dagger\tilde{\boldsymbol{g}} \tag{38}$$

The optimal $\boldsymbol{h}$ must now be evaluated. The new optimisation problem becomes

$$\min_{\boldsymbol{h}} \boldsymbol{h}^\dagger\hat{\tilde{\boldsymbol{\Phi}}}\boldsymbol{h} \tag{39}$$

under the constraint

$$\boldsymbol{h}^\dagger\tilde{\boldsymbol{x}}_{M_s\tilde{M}_d}^{sd} = 1 \tag{40}$$

with

$$\hat{\tilde{\boldsymbol{\Phi}}} = \hat{\tilde{\boldsymbol{\Xi}}} - \tilde{\boldsymbol{g}}\tilde{\boldsymbol{g}}^\dagger \tag{41}$$

This quadratic optimisation problem with a linear equality constraint can be solved using Lagrange multipliers. The solution (when it exists) is

$$\boldsymbol{h} = \frac{\hat{\tilde{\boldsymbol{\Phi}}}^{-1}\tilde{\boldsymbol{x}}_{M_s\tilde{M}_d}^{sd}}{(\tilde{\boldsymbol{x}}_{M_s\tilde{M}_d}^{sd})^\dagger\hat{\tilde{\boldsymbol{\Phi}}}^{-1}\tilde{\boldsymbol{x}}_{M_s\tilde{M}_d}^{sd}} \tag{42}$$

This last equation, in association with (38), provides the optimal solution. □